

To appear in *Astrophysical Journal (Letters)*.

Resolution and Kinematics of Molecular Gas Surrounding the Cloverleaf Quasar at $z=2.6$ Using the Gravitational Lens

M. S. Yun¹, N. Z. Scoville, J. J. Carrasco, & R. D. Blandford
California Institute of Technology, Pasadena, CA 91125

ABSTRACT

Gravitational lenses have long been advertised as primitive telescopes, capable of magnifying cosmologically distant sources (Zwicky 1937). In this Letter, we present new, $0''.9$ resolution CO (7–6) observations of the $z = 2.56$ Cloverleaf quasar (H 1413+117) and spatially resolved images. By modeling the gravitational lens, we infer a size scale of $0''.3$ (~ 1 kpc) for the molecular gas structure surrounding the quasar, and the gas has a kinematic structure roughly consistent with a rotating disk. The observed properties of the CO emitting gas are similar to the nuclear starburst complexes found in the infrared luminous galaxies in the local universe, and metal enrichment by vigorous star formation within this massive nuclear gas complex can explain the abundance of carbon and oxygen in the interstellar medium of this system observed when the universe was only a few billion years old. Obtaining corresponding details in an unlensed object at similar distances would be well beyond the reach of current instruments, and this study highlights the less exploited yet powerful use of a gravitational lens as a natural telescope.

Subject headings: quasars: individual (H 1413+117) — cosmology: observations — galaxies: starburst — ISM: molecules — infrared: galaxies

1. Introduction

The Cloverleaf quasar (H 1413+117) is one the most distant objects where the presence of a large amount of cold, molecular gas is inferred from the detection of bright CO emission (Barvainis et al. 1994). Its spectral energy distribution peaks in the far-infrared as in another luminous high redshift object FSC 10214+4724 ($z=2.29$) (Barvainis et al. 1992, Rowan-Robinson et al. 1993, Eisenhardt et al. 1996), and the total infrared luminosity and inferred molecular gas mass are comparable for these two objects. The optical image consists of four clearly separated

¹present address: National Radio Astronomy Observatory, P.O. Box 0, Socorro, NM 87801, USA (*myun@nrao.edu*)

peaks implying that the (unseen) lens lies close to the line of sight to the quasar (Kayser et al. 1990). While the optical quasar may appear unresolved, the surrounding gas and dust is expected to be substantially extended, and the new CO (7–6) observations are made at $1''$ resolution in order to resolve the distribution of molecular gas complex surrounding the quasar. Previous CO observations at much lower spatial resolutions ($\theta = 3''\text{--}8''$) had failed to resolve the molecular gas structure (Barvainis et al. 1994, Wilner et al. 1995).

In the following sections, we show that the CO (7–6) emission in the Cloverleaf quasar is indeed resolved by our new interferometric observations and demonstrate that $0''.1$ scale spatial details can be revealed by gravitational lensing in addition to the usual luminosity amplification. This magnifying property of gravitational lens holds promise for probing minute details of distant objects unachievable through a conventional observational approaches.

2. Observations and results

Aperture synthesis observations of CO (7–6) emission ($\nu_0 = 806.651776$ GHz) redshifted to 226.70 GHz were carried out at the Owens Valley Millimeter array between December 1994 and March 1995 in the equatorial and high resolution configurations with longest baselines 200 m (E-W) and 220 m (N-S). Typical system temperatures were 500-800 K (SSB), mainly contributed by the atmosphere. A digital correlator configured with 120×4 MHz (5.3 km s^{-1}) channels covered a total velocity range of 636 km s^{-1} . The data were calibrated using the standard Owens Valley array program MMA (Scoville et al. 1992), and the continuum and spectral line maps are made with DIFMAP (Shepherd et al. 1994). Data from total of 30 baseline pairs cover the inner 12-180 $k\lambda$ uv-plane, and the resulting synthesized beam is $0''.86 \times 1''.0$ (PA= 73°) with natural weighting of the visibility data. The uv-coverage is quite uniform, and synthesized beam is well-behaved – the largest sidelobes appear $2''$ north and south of the main beam with 20% of the peak amplitude. The CLEANing of the maps was limited only to the central $3''$ diameter region - no emission is seen elsewhere in the “dirty” maps. The positional accuracy of the resulting maps is better than $0''.2$. After 25 hours of on-source integration, we achieved 3.2 (LSB) and 4.9 (USB) mJy beam $^{-1}$ sensitivity in the 1 GHz bandwidth analog correlator continuum data. The CO (7–6) emission appears in only 1/2 of the total 120 spectrometer channels, and 1σ noise in each 110 MHz ($\Delta V = 145 \text{ km s}^{-1}$) averaged channel maps (Figures 1b & 1c) is 8.3 mJy beam $^{-1}$. No continuum emission is detected in the 230 GHz USB continuum data, and the 3σ upper limit of 15 mJy beam $^{-1}$ is marginally consistent with the 240 GHz continuum flux of 18 ± 2 mJy reported by Barvainis et al. (1995). The summary of the observations and results are given in Table 1.

The new CO (7–6) map resolves the source for the first time (Fig. 1). The velocity integrated CO emission, Figure 1a, approximately follows the optical light suggesting that the CO source is close to the quasar. However, the peak of the CO emission is located near image B, whereas image A is the brightest in the optical and infrared – perhaps a first hint that the distribution of the CO emission is different from that of the quasar light. Since the CO emission does not form an

Einstein ring (c.f., MG 1131+0456, Hewitt et al. 1988), the CO emitting region must be smaller in size than that of the tangential caustic, $\sim 1''$ or about $4 h^{-1}$ kpc (assuming that $\Omega_o = 1$). Our integrated CO (7–6) spectrum has the same profile as the IRAM 30-m spectrum (R. Barvainis, private communication), and it is not shown because of the space limitation in this *Letter*.

In order to study the kinematics of the gas, we produced separate images of the blue- and redshifted gas (Fig. 1c & 1d). Clear differences from the optical image are seen in both the blue- and the redshifted images while the difference between the two is also significant as shown in Fig. 1b. Thus two kinematically distinct sources have been spatially resolved by the gravitational lens. As in the velocity integrated image (Fig. 1a), the blue- and redshifted gas images also have multiple bright peaks but spatially displaced from each other and from the optical quasar positions. This displacement is quite significant, each ~ 7 times the rms noise in the maps. Because the position information depends on the phase of the visibilities, which is measured much more accurately than amplitude by an interferometer, the significance of the offset is even greater. In addition, the fact that the multiple peaks in both blue and redshifted CO images can be mapped back to single distinct (but different) features in the source plane further supports the reality of observed differences (see below).

Comparison of our data with unpublished Plateau de Bure (PdB) interferometer maps (R. Antonucci & R. Barvainis, private communication) also lends support to the extended nature of the CO emission. The higher resolution PdB maps show a 3-image geometry for the CO emission, similar to our own, but observed differences as function of velocity are much less pronounced. The total line flux mapped by the PdB interferometer is about 25% less than our measurement, and their uv-coverage poorly samples the baselines shorter than 50-m in length (needed to map 2-3'' scale structures). Only 30% of the total flux is seen in the difference map (Fig. 1b), and thus one may infer that about 70% of the line flux originates in a very compact region, very close to the quasar, while the remaining 30% lies further out, if the both observations are accurate.

3. Gravitational Lensing Model and Inferences

In order to test our hypothesis that the observed difference between the blue and red CO images is due to spatial resolution of the gas distribution and kinematics, we have developed a gravitational lens model. We have modeled the lens as a single elliptical potential with an external shear (Schneider et al. 1992)

$$\psi = b[1 + (1 - \gamma_c)(x/s)^2 - 2\gamma_s(xy/s^2) + (1 + \gamma_c)(y/s)^2]^q - \gamma_1(x^2 - y^2) - 2\gamma_2xy$$

where b measures the size of the Einstein ring and s is a core radius. The parameters $\gamma_{c,s}$ represent the ellipticity in the galaxy potential and the parameters $\gamma_{1,2}$ measure the strength of the tidal action of external galaxies. The exponent q is dictated by the radial density profile. A value $q = 0.5$ corresponds to the (pseudo-)isothermal case. We solved for parameters which reproduce the HST image locations (Falco 1993) and which also recover the three relative magnifications

of the four K band images measured nearly contemporaneously with the Keck telescope (M. Pahre, private communication). These relative magnifications are quite similar to their optical counterparts. We take this as an indication that microlensing is unimportant. For an emitted wavelength ~ 600 nm, a thermal source would be too large to be treated as a point source when microlensed by $\sim 0.1 M_{\odot}$ stars in an intervening galaxy (cf. Rauch & Blandford 1991). A non-thermal, red source could, however, be subject to strong, achromatic microlensing and if this is happening, our model would definitely be invalid. High accuracy photometric monitoring may determine if microlensing is at work. (In a different approach to modeling this source, Kayser et al (1990) invoke microlensing and ignore the measured magnifications in deriving a macrolensing model. They present two quite different models that fit the image locations; one involves a single galaxy with eccentricity larger than 0.9, the other uses two galaxies. Neither model is compatible with our CO data – see below.)

Our model is able to reproduce both the image locations and relative fluxes to within the measurement accuracies. The best fitting parameters are $b = 0.088''^2$, $s = 0.21''$, $\gamma_c = 0.09$, $\gamma_s = 0.15$, $q = 0.61$, $\gamma_1 = -0.05$, $\gamma_2 = -0.08$. The lensing galaxy is centered at $(-0.13'', +0.56'')$ relative to image A. The corresponding ellipticity in the surface density contours is $\epsilon = 0.3$, and the position angle of its major axis is 125° (see Figure 2a). This model is quite different from the single galaxy model of Kayser et al. It is roughly orthogonal in orientation and much less elliptical. The total point source magnification $\mu = 220$ is much larger than the Kayser et al model implying that the source is correspondingly less powerful. It also implies that the time delays are very much shorter. Adopting $z_d = \Omega_0 = 1$, for example, we obtain $t_{BA} = -0.3$, $t_{CA} = -0.5$, $t_{DA} = 0.9 h^{-1}$ day, which will be a challenge to measure. We have preferred this model because it seems best able to accommodate the CO data. However, as the foregoing discussion implies, it is not unique and much more will need to be known before this source becomes a good candidate for determining the Hubble constant.

We now adopt this lens model and use it to derive CO source models that provide the best fit to the red and the blue images. Using the adopted lens model, we were able to produce an excellent fit to the contours of the redshifted CO image; the fit to the blueshifted image was less good but acceptable granted the resolution of the observation (Fig. 2b & 2c). We find that the peaks of the red and the blue source are displaced by $\sim 0''.15 \equiv 550h^{-1}$ pc with respect to the quasar, roughly on opposite sides of the optical source. This suggests that the molecular gas orbits the quasar. We obtain a dynamical estimate of the central mass of $\sim 10^{10}h^{-1} M_{\odot}$ adopting a low inclination $i \sim 30^{\circ}$, on the grounds that H 1413+117 is a broad absorption line (BAL) quasar. (Note, though, that the quasar is not being observed through the molecular gas as the high extinction $A_v > 1000$ would render it optically invisible.) The fact that each of the multiply imaged CO sources, each with $\sim 7\sigma$ in significance, map back to a *single* image on opposite side of the quasar gives us additional confidence in our modeling and the reality of the observed differences between the red and blue images. The two CO sources are not exactly symmetric about the quasar, and this may reflect a real asymmetry in the gas distribution, an error in relative astrometry between optical

and CO images ($\lesssim 0.''2$), or an inaccuracy in the lens model.

The overall CO magnification depends on the source size (Eisenhardt et al. 1996). For our predicted overall CO source size, we estimate that the mean magnification is $\mu_{CO} \sim 10$. A similar magnification is probably appropriate for the far infrared emission discussed below. Adopting this value, the associated molecular gas mass is calculated from the observed flux ($S_{CO(7-6)} = 41 \text{ Jy km s}^{-1}$) to be $\sim 2 \times 10^{10} h^{-2} M_{\odot}$ using a standard Galactic CO-to-H₂ conversion factor (Young & Scoville 1991, Solomon et al. 1992). A lower than solar metallicity requires a somewhat larger gas mass to account for the observed CO flux. Because of the small source size ($\lesssim 3''$), our interferometer measurement should include all the emission – the existing single dish measurement of CO (7–6) flux is quite uncertain because it suffers from lack of a good spectral baseline (R. Barvainis, private communication). This inferred mass of molecular gas is comparable with the upper bound derived on the basis of dynamics, and we therefore suppose that it is a fair estimate of the total molecular hydrogen mass. This in turn implies that molecular gas may dominate the mass distribution on the $\sim 1 \text{ kpc}$ scale just as in the ultraluminous infrared galaxies in the local universe (Scoville & Soifer 1991, Yun & Scoville 1995, Bryant & Scoville 1996).

4. Physical Properties of the Molecular Gas Surrounding the Quasar

The CO emitting gas appears to be both warm and dense. The peak observed brightness temperature for the CO (7–6) line seen in the individual 32 MHz channel maps is 2.2 K above the brightness temperature of the cosmic background radiation. Gravitational lensing preserves brightness temperature, and this excess corresponds to a Planck brightness temperature at the source redshift of 24 K. If the lensed image fills 1/2 (1/4) of the synthesized beam, then the inferred temperature of the gas is about 50 (100) K. The CO (7–6) line is bright, and the near unity (~ 0.9) inferred brightness temperature ratio of our CO (7–6) measurement to that of the CO (3–2) measurement by Barvainis et al. (1994) suggests that the CO emitting gas is thermalized and optically thick if both transitions originate from the same region. (In support of this, we note that both transitions have the same line width and profile.) Because the CO $J = 7$ rotational level lies 155 K above the ground state, producing significant CO (7–6) emission and the observed line ratio requires a minimum density of $n > 10^5 \text{ cm}^{-3}$ and an excitation temperature $T_{ex} \gtrsim 100 \text{ K}$. The inferred dust temperature from the continuum spectrum is $\sim 100 \text{ K}$ (Barvainis et al. 1992, Downes et al. 1992, Rowan-Robinson et al. 1993), and this is consistent with the expectation that the dust and gas should be in thermal equilibrium at the density required for producing the observed CO (7–6) flux. The observed spectral energy distribution for the infrared and submillimeter emission can be interpreted as thermal emission from dust with total mass of $\sim 5 \times 10^7 M_{\odot}$, which corresponds to a gas mass $2.5 \times 10^{10} M_{\odot}$ after correcting for the lens magnification and adopting a gas to dust ratio ~ 500 appropriate to infrared galaxies in the local universe (Sanders et al. 1991). This is in good agreement with the gas mass estimate from the CO emission above although large uncertainties are associated with both estimates.

The infrared luminosity to molecular gas ratio L_{FIR}/M_{H_2} is a crude measure of the efficiency of converting gas into radiant energy either through stars or via an active nucleus. Among the most luminous infrared galaxies found in the local universe, this ratio approaches $\sim 100 L_{\odot}/M_{\odot}$. However, for H 1413+117 and FSC 10214+4724, the observed ratios exceed $200 L_{\odot}/M_{\odot}$ (neglecting the possibility of different magnification for the infrared and CO emission). This suggests that the bulk of the large infrared luminosities of both of these objects is provided by a quasar, that is hidden in the case of FSC 10214+4724. In these discussions, it is assumed that the CO emitting region coincides with the infrared emitting region because a large amount of dust associated with the CO emitting dense molecular gas would dominate the total infrared emission.

In summary, we note that the molecular gas complex in H 1413+117 is similar in size, mass, density, and temperature, to that observed in the nuclei of local infrared galaxies (Sanders et al. 1991). This is consistent with theoretical models in which a large quantity of gas driven into the nuclear region by mergers or interactions (Barnes & Hernquist 1991) is processed by starbursts over a time scale $\sim 10^8$ years so that it builds up a high metallicity (Scoville & Soifer 1991). This process may account for the strong CO emission from the ISM of this $z=2.6$ system observed when the universe was only a few billion years old.

Here we have also demonstrated that gravitational lens indeed can be a valuable tools for probing objects at cosmological distances by yielding details that are normally inaccessible for the current generation of observational instruments. For example, the resolution of the distribution and kinematics of the massive molecular gas complex surrounding a similarly distant unlensed quasar would require a ten fold improvement both in resolution and sensitivity over the existing instruments. Over 20 gravitationally lensed objects suitable for detailed studies using this gravitational lens telescope are now known in the literature (see Blandford & Narayan 1992, Maoz et al. 1993, King & Browne 1996), and studies exploiting this magnifying characteristic at all wavelengths may be rewarded with valuable new insights on these distance sources.

The authors are grateful to E. Falco for kindly providing the HST image for the analysis and comparison and R. Barvainis for sharing his unpublished data. This manuscript also benefitted greatly from the careful reading and useful suggestions by P. Ho and referee R. Antonucci. This research is supported in part by NSF Grant AST 93-14079.

REFERENCES

- Barnes, J. E., & Hernquist, L. E. 1991, ApJ, 370, L65
- Barvainis, R., Antonucci, R., Hurt, T., Coleman, P., & Reuter, H.-P. 1995, ApJ, 451, L9
- Barvainis, R., Tacconi, L., R., Antonucci, R., Alloin, D. & Coleman, P. 1994, Nature, 371, 586
- Barvainis, R., Antonucci, R., & Coleman, P. 1992, ApJ, 399, L19
- Blandford, R. D., & Narayan, R. 1992, ARAA, 30, 311
- Bryant, P. M. & Scoville, N. Z. 1996, ApJ, 457, 678
- Downes, D., Radford, S.J.E., Greve, A., Thum, C., Solomon, P. M. & Wink, J. E. 1992, ApJ, 398, L25
- Eisenhardt, P. R., Armus, L., Hogg, D. W., Soifer, B. T., Neugebauer, G. et al. 1996, ApJ, 461, 72
- Falco, E. E. 1993, in *Gravitational Lenses in the Universe*, eds. Surdej et al., (Université de Liège, Liège), 127
- Hewitt, J. N., Turner, E. L., Schneider, D. P., Burke, B. F., Langston, G. I., & Lawrence, C. R. 1988, Nature, 333, 537
- Kayser, R., Surdej, J., Condon, J. J., Kellermann, K. I., Magain, P., Remy, M., & Smette, A. 1990, ApJ, 364, 15
- King, L. J., & Browne, I. W. A. 1996, MNRAS, 282, 67
- Magain, P., Surdej, J., Swings, J.-P., Borgeest, U., Kayser, R., Kuhr, H., Refsdal, S. & Remy, M. 1988, Nature, 334, 325
- Maoz, D., Bahcall, J. N., Schneider, D. P., Bahcall, N. A., Djorgovski, S., Doxsey, R., Gould, A., Kirhakos, S., Meylan, G., Yanny, B. 1993, ApJ, 409, 28
- Rauch, K. P., & Blandford, R. D. 1991, ApJ, 381, L39
- Rowan-Robinson, M. et al. 1993, MNRAS, 261, 513
- Sanders, D. B, Scoville, N. Z., & Soifer, B. T. 1991, ApJ, 370, 158
- Schneider, P., Ehlers, J., & Falco, E. E. 1992, *Gravitational Lenses* (Springer-Verlag, Berlin).
- Scoville, N.Z., Carlstrom, J.C., Chandler, C.J., Phillips, J.A., Scott, S.L., Tilanus, R.P., & Wang, Z. 1992, PASP, 105, 1482
- Scoville, N. Z., Sargent, A. I., Sanders, D. B., & Soifer, B. T. 1991, ApJ, 366, L5

Scoville, N. Z., & Soifer, B. T. 1991, in *Massive Stars and Starburst*, ed. K. Leitherer, (Cambridge Univ. Press, Cambridge), 233

Shepherd, M.C., Pearson, T.J., & Taylor, G.B. 1994, *BAAS*, 26, 987

Solomon, P. M., Downes, D., & Radford, S. J. E. 1992, *ApJ*, 387, L55

Wilner, D. J., Zhao, J.-H., & Ho, P.T.P. 1995, *ApJ*, 453, L91

Young, J. S., & Scoville, N. Z. 1991, *ARAA*, 29, 581

Yun, M. S., & Scoville, N. Z. 1995, *ApJ*, 451, L45

Zwicky, F. 1937, *Phys. Rev.*, 51, 290

Table 1. Summary of the Observations

RA (B1950)	$14^h 13^m 20^s.08$
Dec (B1950)	$11^\circ 43' 37''.8$
ν_{obs}	226.7035 GHz
$\langle z_{CO(7-6)} \rangle$	2.5582 ± 0.0003
Luminosity Distance, D_L^a	$10.2 h^{-1} \text{ Gpc}$
Angular Size Distance, D_A^b	$0.79 h^{-1} \text{ Gpc}$ ($1'' = 3.8 h^{-1} \text{ kpc}$)
θ_{FWHM}	$0''.86 \times 1''.0 \text{ (PA} = 73^\circ)$
$(\Delta V)_{FWHM}$	$339 \pm 21 \text{ km s}^{-1}$
$S_{CO}\Delta V$	$41 \pm 4 \text{ Jy km s}^{-1}$
$L_{CO(7-6)} (=4\pi D_L^2 S \Delta V \nu_{obs})$	$5.5 \times 10^8 h^{-1} L_\odot$
M_{H_2}	$2.5 \times 10^{10} h^{-2} M_\odot \text{ (for } \mu = 10)$
M_{dyn}	$2.6 \times 10^{10} [R(\text{kpc})]^{-1} (\text{Sin } i)^{-2} M_\odot$

^a $D_L = 6000 [(1+z) - (1+z)^{1/2}] h^{-1} \text{ Mpc}$ (for $\Omega_o = 1$)

^b $D_A = D_L/(1+z)^2$.

Fig. 1.— **(a)** Velocity integrated map of CO (7–6) emission from the Cloverleaf quasar (H 1413+117) at $0''.86 \times 1''.0$ (PA= 73°) resolution in contours overlaid on the gray scale optical image obtained with the Hubble Space Telescope (Falco 1993). The contours are -3, -2, 2, 3, 4, 5, 6, 7, 8, and 9 times the rms noise ($5.3 \text{ mJy beam}^{-1}$). Image “A” is brightest in optical light, but the CO peaks near image “B”, probably reflecting real differences in the underlying distributions. The coordinates are in offset with respect to image A. **(b)** A difference map between the blue and redshifted emission [shown in (c)&(d)] made in order to test if the two velocity components are resolved. The contour levels are the same as in (c)&(d) for a direct comparison. **(c)&(d)** Blue- and redshifted CO (7–6) emission averaged over 145 km s^{-1} are shown in contours superposed on the HST image. The contours are -3, -2, 2, 3, 4, 5, and 6 times the rms noise ($8.3 \text{ mJy beam}^{-1}$). The blue and red images consist of 2-3 bright peaks, each with distinctly different distribution from the other and from the optical light. While the apparent difference in morphology between the blue and red image is striking, only 30% of the total flux remains in the difference map, suggesting that the bulk of the flux originates very close to the quasar.

Fig. 2.— **(a)** Evenly-spaced contours of surface mass density in a simple elliptical potential plus external shear gravitational lens model computed to account for the observed locations and relative magnifications of the optical/infrared images. The star marks the location of the lensed quasar. (The apparent higher brightness of optical image B over A is an artifact of re-gridding poorly sampled HST image.) **(b)&(c)** Blue- and redshifted CO source models produced by ray-tracing observed CO images through the lens model and convolving with a $0''.2$ beam corresponding to the effective resolution of the gravitational lens. The contours are linear increments of the 15% of the peak brightness. The red and blue CO sources are located roughly on the opposite side of the quasar, each located $\sim 0''.15$ ($550h^{-1} \text{ pc}$) away, and the observed distribution may be interpreted as the CO emitting region having about 1 kpc in extent with a velocity gradient like a rotating disk.

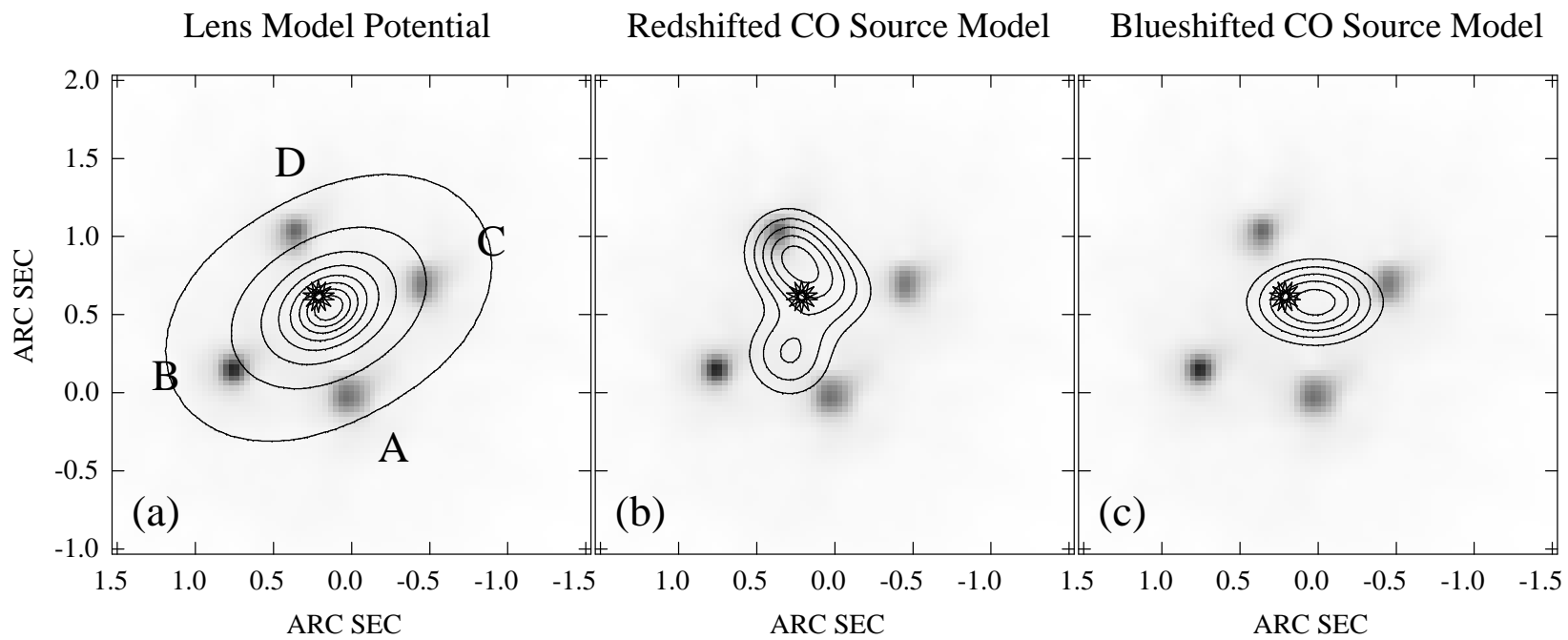


Figure 2.